High-resolution hard X-ray phase-contrast microscopy with a large-diameter and high-numerical-aperture zone plate

Yasushi Kagoshima,[a]* Yoshiyuki Yokoyama,[a] Takashi Ibuki,[a] Toshihiro Niimi,[a] Yoshiyuki Tsusaka,[a] Kengo Takai[b] and Junji Matsui[a]

[a]Faculty of Science, Himeji Institute of Technology, 3-2-1 Kouto, Kamigori, Ako, Hyogo 678-1297, Japan, and [b]Japan Synchrotron Radiation Research Institute, 1-1-1 Kouto, Mikazuki, Sayo, Hyogo 679-5198, Japan.
E-mail: kagosima@sci.himeji-tech.ac.jp

An imaging transmission hard X-ray microscope has been constructed at beamline BL24XU of SPring-8. It makes use of a phase zone plate made of tantalum with a diameter of 1 mm and an outermost zone width of 50 nm, aiming at a wide field of view and a high spatial resolution. The performance test was carried out at a photon energy of 10 keV. A field of view as wide as ~200 µm in diameter was achieved. The spatial resolution was measured to be 220 nm by analyzing a knife-edge image. Further, a line-and-space pattern as fine as 100 nm could be imaged. By placing a phase plate made of gold in the back focal plane of the zone plate, phase-contrast microscopy using Zernike's method was also carried out. The feasibility of phase-contrast microscopy for observing transparent samples was successfully demonstrated by imaging small polystyrene particles.

Keywords: X-ray microscopes; zone plates; high resolution; phase contrast.

1. Introduction

Hard X-rays have unique properties as probes in microscopy for studying biological specimens, for example, the ability to image thick specimens in their natural living state, the easy preparations of specimens and the non-destructive observation under an atmospheric environment. In particular, in the case of an imaging transmission microscope, Zernike's phase-contrast microscopy will be effective because δ for light elements is almost 1000 times larger than β in the hard X-ray region, where δ is the deviation of the real part of the refractive index from unity and β is the imaginary part of the refractive index. Although several hard X-ray imaging transmission microscopes have been demonstrated (Snigirev, 1995; Lai et al., 1995; Lengeler et al., 1999; Kohmura et al., 1999, 2001; Leitenberger et al., 2000), only a few microscopes using Zernike's method have been applied to samples composed of light elements (Watanabe et al., 2000; Kagoshima et al., 2001). In this paper, we demonstrate the feasibility of Zernike's phase-contrast microscopy for observing transparent samples of light elements. Further, the wide field of view and the high spatial resolution are also demonstrated by using a phase zone plate having a large diameter and high numerical aperture.

2. Optical system

An imaging transmission hard X-ray microscope was constructed at beamline BL24XU of SPring-8. Details of the beamline BL24XU are given elsewhere (Tsusaka et al., 2001). The optical system of the microscope is shown in Fig. 1. The photon energy of the fundamental harmonic peak of the undulator was tuned to 10 keV. The X-ray beam was first collimated by a four-quadrant slit, of both height and width 1 mm, placed at a distance of 30 m from the light source point (not shown in Fig. 1). Then the beam was monochromatized using a horizontal-dispersion silicon double-crystal monochromator with 111 Bragg reflections. Quasi-parallel beam illumination was employed in order to make the optical system simple, although a critical illumination system consisting of a condenser zone plate and a pinhole was employed in our previously reported X-ray microscope (Kagoshima et al., 2000). Owing to the nature of the zone plate, an off-axis arrangement must be taken in the case of parallel beam illumination so that the desired real image can be spatially separated from undesired images produced by diffraction orders of the zone plate other than the +1st order, as shown in Fig. 1. For the off-axis arrangement a lead plate was placed in front of the object. The distance between the edge of the lead plate and the beam axis was 100 µm. The zone plate formed the real image in an image plane. The off-axis arrangement in a zone plate microscope has been analyzed in detail elsewhere (Kagoshima et al., 1990) and recently followed by two groups (Leitenberger et al., 2000; Kaulich et al., 1999). For phase-contrast microscopy, a phase plate was placed in the back focal plane of the zone plate objective. Since the high coherence of the undulator radiation is harmful in the case of imaging microscopes, a diffuser can be inserted in front of the lead plate in order to decrease the coherence of illumination. Diffusers for this purpose have already been used in the soft X-ray (White et al., 1995) and hard X-ray (Awaji et al., 2001) regions. The optical magnification was limited to ×9.5 at
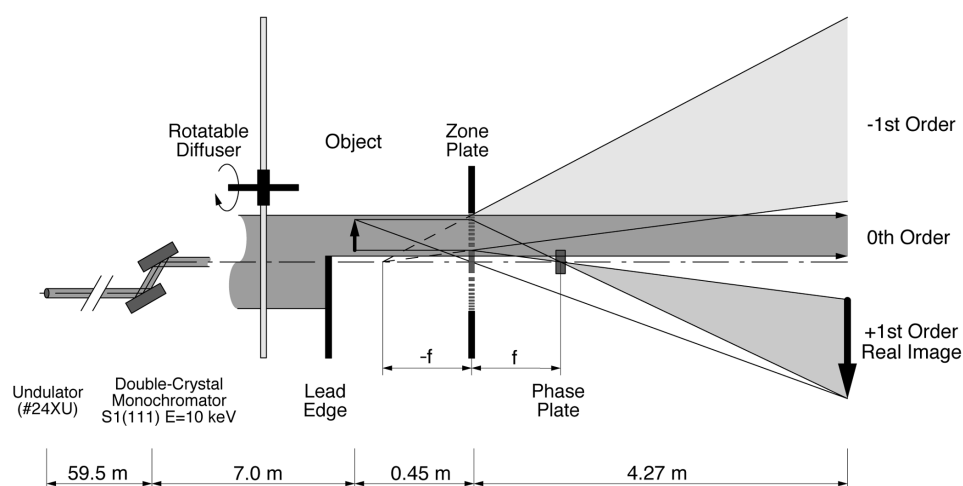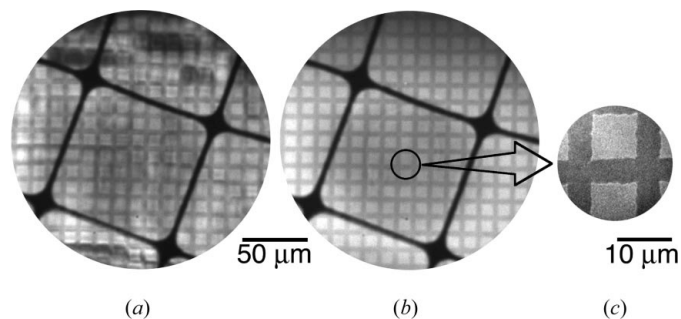

Figure 1
Optical system of the imaging transmission hard X-ray microscope constructed at BL24XU of SPring-8. The microscope used quasi-parallel beam illumination. The photon energy used was 10 keV. A zone plate of diameter 1 mm and an outermost zone width of 50 nm was used as an objective X-ray lens. In order to spatially separate the desired +1st order real image, a lead plate was placed in front of the sample. A rotatable diffuser was inserted in front of the lead plate in order to decrease the coherence of illumination. In the case of phase-contrast microscopy, a phase plate was placed in the back focal plane of the zone plate objective. The optical magnification of the microscope was ×9.5.

10 keV by the finite space inside the experimental hutch. By employing an X-ray zooming tube (Kinoshita *et al.*, 1992), of which the spatial resolution was evaluated to be 0.74 µm at a photon energy of 8 keV (Takano *et al.*, 2001), as an X-ray imaging device, a spatial resolution of approximately 80 nm could be achieved by the total system.

The zone plate used as the objective X-ray lens was fabricated by NTT Advance Technology Corporation and made of tantalum (Ozawa *et al.*, 1997). Its relevant parameters are as follows: the radius of the innermost zone (r_1) is 7.07 µm, the number of zones (N) is 5000, the outer diameter (D) is 1 mm, and the width of the outermost zone (δr_N) is 50 nm. The focal length and the numerical aperture are 40 cm and 1.24×10^{-3} at 10 keV, respectively. The thickness of tantalum is 350 nm, which gives a theoretical diffraction efficiency of 1.5%. Although the value seems small, the zone plate still functions well as a lens as will be shown later. The zone plate requires the condition that the monochromaticity of illumination, $\Delta E/E$, should be smaller than the inverse of the number of zones, namely $1/N$, in order to eliminate the chromatic aberration. In the present case, the condition is that $\Delta E/E \leq 1/N = 2 \times 10^{-4}$. Since the monochromaticity of the present system was estimated to be 2.1×10^{-4} (Kagoshima *et al.*, 2000), the condition was almost satisfied and therefore the chromatic aberration could be negligible.

3. Effect of diffuser

As mentioned in the previous section, a diffuser was introduced in order to decrease the coherence of illumination. Without the diffuser, the high coherence of the undulator radiation disturbed the image field, and therefore neither wide nor uniform illumination could be ensured. The diffuser used was made of diamond paste. The size of the diamond powder particles in the paste was 6 µm. A kapton film on which the diamond paste was painted was mounted on a small metal wheel. The wheel was placed perpendicularly to the beam axis and could be rotated by a DC motor as shown in Fig. 1. The diffuser had a thickness equivalent to approximately 30 µm of diamond. The value of 30 µm was estimated by measuring the transmission of the diffuser at 10 keV. The diffuser was rotated during the exposure in order to average the thickness ununiformity of the diamond paste. Fig. 2 demonstrates the effect of the diffuser, where the sample was a copper #2000 mesh. Without the diffuser the illumination is not uniform and the mesh patterns are disturbed due to the highly
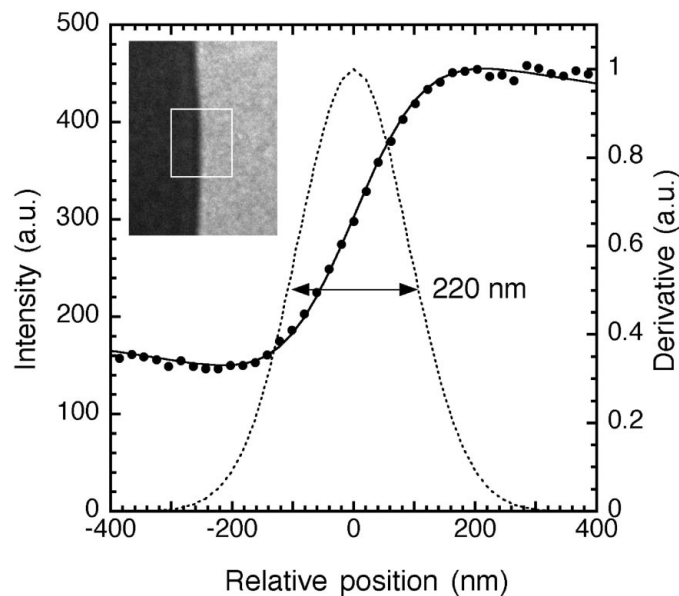

Figure 2
Magnified images of a copper #2000 mesh demonstrating the effect of the diffuser: (*a*) without the diffuser and (*b*) with the diffuser. In (*a*) the illumination is not uniform, while in (*b*) uniform illumination of approximately 200 µm in diameter can be achieved. The large thick mesh is for supporting a photoelectric membrane of the zooming tube. A zoomed-up image (*c*) demonstrates the good spatial resolution. The magnification of the zooming tube was ×10 for (*a*) and (*b*), and ×100 for (*c*). The exposure time was 50 s for (*a*) and (*b*), and 5 min for (*c*).

coherent property of the undulator radiation, while with the diffuser a uniform illumination of approximately 200 µm in diameter can be achieved. Since the distance between the edge of the lead plate and the optical axis was 100 µm, the off-axis distance, namely the distance between the optical axis and the center of the image filed, was 200 µm. The result shows that the diffuser functioned well to achieve the wide and uniform illumination.

To discuss the effect of the diffuser correctly, the angular divergence of the incident beam and the spot size in the back focal plane are very important. The spot size was measured by the knife-edge method and it was enlarged by the diffuser from 2.3 µm to 3.5 µm in the vertical direction and from 10.6 µm to 15.8 µm in the horizontal direction. The difference between the vertical and the horizontal directions are mainly due to the source size. As will be seen later, the difference does not affect the imaging properties of the optical system. The angular divergence of the incident beam has not yet been measured. It will be measured in the near future.

4. Performance test

The spatial resolution was evaluated by the knife-edge method. As a knife edge, a 4 µm-thick tantalum edge structure deposited on an SiN membrane was used. A magnified image of an edge pattern is shown as an inset in Fig. 3. The edge response was analyzed and the result is shown in Fig. 3. The raw data were fitted with an error function assuming a uniform background. Taking the derivative of the fitted curve, the line spread function was obtained as a Gaussian function. Since the full width at half-maximum of the line spread function corresponds to the spatial resolution, that of the microscope was evaluated to be 220 nm. Further, another zone plate made of tantalum with a thickness of 0.6 µm was also used as a test line-and-space pattern. Fig. 4 shows a magnified image of the outermost region
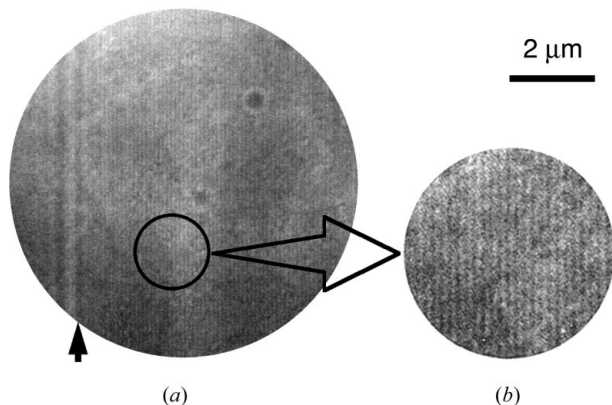

Figure 3
Measured edge response (dots), the fitted curve with an error function assuming a uniform background (solid line) and the derivative of the fitted curve (dashed line) are shown. The FWHM of the derivative was evaluated to be 220 nm, which corresponds to the spatial resolution of the microscope. The inset is a magnified image of an edge structure. The dots are averaged values inside the white rectangle in the magnified image. The image was recorded with the diffuser. The magnification of the zooming tube was ×100 and the exposure time was 10 min.

of the sample zone plate. Although the contrast is not sufficiently high, a line-and-space pattern as fine as 100 nm can be imaged with the microscope. This is the finest line-and-space pattern ever obtained with a photon energy as high as 10 keV. The image was recorded without the diffuser because the 100 nm line-and-space pattern could not be imaged when the diffuser was inserted. Fundamentally, if the object is perfect, the spatial resolution will be improved by introducing the diffuser because the coherence of illumination decreases. Therefore, the diffuser somehow reduced the spatial resolution due to its unexpected effects. The reason why the spatial resolution is reduced by the diffuser is under investigation.

As is well known, the spatial resolution of the microscope, Δ, with entirely incoherent illumination can be given by $\Delta \simeq 1.22 \delta r_N$ in the case of the zone plate. In our microscope, the coherence of illumination is not certain at present, but it must be partially coherent. Therefore, the expected spatial resolution should be between $1.22 \delta r_N$ and $2 \delta r_N$. Since δr_N is 50 nm in the present case, a spatial resolution of approximately 60–100 nm can be expected. The experimental resolution is poor, however, in comparison with the expected value. One possible reason for this is the structural imperfection of the zone plate used. Even with the optical microscope, the systematic artifact due to the fabrication error can be observed in the outer region of the zone plate. If it is assumed that the outer region does not contribute to the imaging, the experimental spatial resolution seems reasonable.

5. Phase-contrast microscopy

The principle of Zernike's method is that phase changes introduced by an object are transformed into changes in intensity by shifting (retarding or advancing) the phase of the central order with respect to the diffraction spectra in the back focal plane of the objective (Born & Wolf, 1986). A phase plate that is placed in the back focal plane of the objective shifts the phase of the central order by one-quarter of a period. The theory of phase-contrast microscopy by Zernike's method for X-rays has been well described by Rudolph *et al.* (1990), who first extended the phase-contrast microscopy to the soft X-ray region (Schmahl *et al.*, 1995). We have recently extended it to the hard X-ray region and succeeded in imaging biological specimens in reverse contrast with phase plates to shift the phase by one-quarter and three-quarters of a period (Kagoshima *et al.*, 2001), where critical illumination was employed and the spatial resolution

was approximately 500 nm. In the present paper, we chose a quasi-parallel beam illumination and therefore the phase plate should have a disc shape. The phase plate was made of gold and the thickness was designed to be 1.0 μm in order to shift the phase by one-quarter of a period at 10 keV. For making the phase plate, a pinhole of diameter 20 μm was placed on a kapton film, and gold was deposited on it. After deposition, the pinhole was removed from the kapton film. The diameter of the phase plate was approximately 24 μm. Although the diameter was larger than the measured spot size of the central order in the back focal plane of the zone plate, as described in §3, the phase plate worked well as shown below.

We first attempted to image a metal sample. Fig. 5 shows magnified images of a copper #2000 mesh. Fig. 5(*a*) shows an absorption-contrast image (taken *without* the phase plate) and Fig. 5(*b*) shows a phase-contrast image (taken *with* the phase plate). Completely different image contrast appeared in the two images. For example, contours of the mesh pattern are emphasized by reduction of intensity; in other words, black lines edge the mesh pattern. Further, since copper mesh parts are slightly brighter than the background in Fig. 5(*b*), the image contrast is in the reverse relationship between the two images. The images demonstrate that phase-contrast microscopy provides different information in comparison with the usual absorption-contrast imaging, even for metal samples.

Next, we attempted to image a sample of light elements. Fig. 6 shows magnified images of polystyrene particles with a particle size of 7 μm. Fig. 6(*a*) shows an absorption-contrast image (taken *without* the phase plate) and Fig. 6(*b*) shows a phase-contrast image (taken *with* the phase plate). Particle structures are clearly imaged with a good contrast in the phase-contrast image of Fig. 6(*b*), while little image contrast is seen in the absorption-contrast image of Fig. 6(*a*). Further, the image contrast is the positive contrast; namely, the larger the optical thickness of the sample, the brighter the image. Since the positive contrast is obtained when the phase of the central order is shifted by one-quarter of a period (Rudolph *et al.*, 1990; Kagoshima *et al.*, 2001), the result is consistent with the theory. Using an equation for phase-contrast microscopy given in our recent paper (Kagoshima *et al.*, 2001), an image contrast of 59% in the case of the positive contrast can be expected at 10 keV for a 7 μm-thick polystyrene layer in an air background. In the calculation, the elemental composition and the density of polystyrene are assumed to be $CH(C_6H_5)CH_2$ and 1.1 g cm^{-3}, respectively. For comparison, the expected absorption contrast is 0.07% at 10 keV. The optical constants used in the calculations were taken from Henke *et al.* (1993). Fig. 7 shows the intensity profile of the polystyrene image in Fig. 6(*b*). The intensity
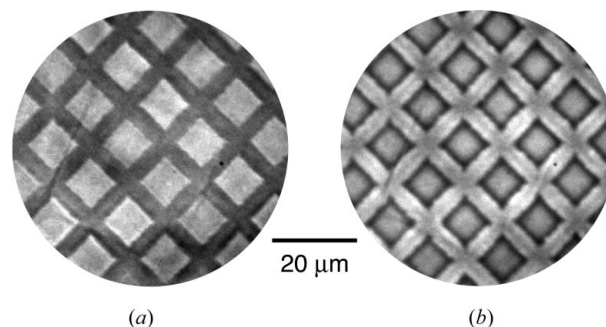

(*a*) (*b*)

Figure 4
Magnified image of the outermost region of the sample zone plate. A line-and-space pattern as fine as 100 nm can be imaged. The image was taken without the diffuser. The left-most zone in (*a*) corresponds to the outermost zone of the sample zone plate (indicated by a solid arrow). The magnification of the zooming tube was ×100 and the exposure time was 10 min.

(*a*) (*b*)

Figure 5
Magnified images of a copper #2000 mesh: (*a*) absorption-contrast image (taken *without* the phase plate) and (*b*) phase-contrast image (taken *with* the phase plate). Both images were recorded with the diffuser. Completely different image contrast appeared in the two images. The magnification of the zooming tube was ×30 and the exposure time was 5 min.
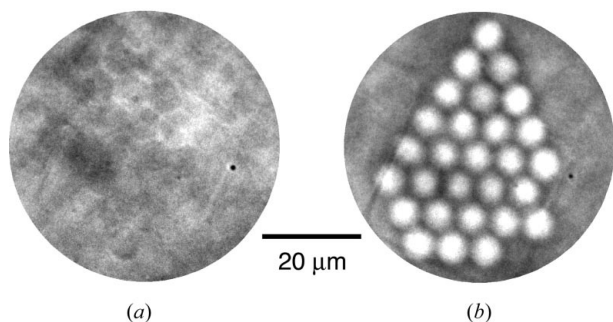
Figure 6
Magnified images of polystyrene particles with a particle size of 7 µm: (*a*) absorption-contrast image (taken *without* the phase plate) and (*b*) phase-contrast image (taken *with* the phase plate). Both images were recorded with the diffuser. Particle structures are clearly imaged with good contrast in the phase-contrast image of (*b*), while little image contrast is seen in the absorption-contrast image of (*a*). The magnification of the zooming tube was ×30 and the exposure time was 5 min.
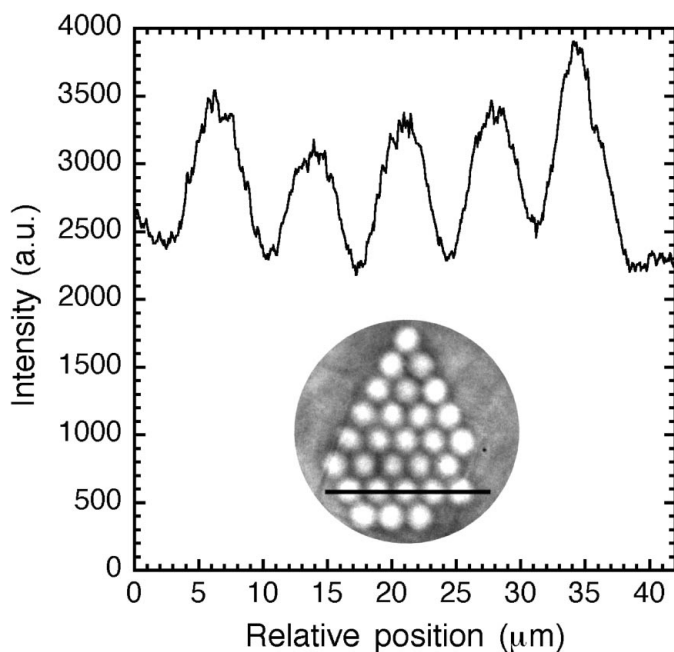
Figure 7
Intensity profile of the polystyrene image in Fig. 6(*b*). The intensity was measured along a black line drawn in the inset image in the graph. The image contrast of the polystyrene particles was estimated to be approximately 20%.

was measured along a black line drawn in the inset image in Fig. 7. From the intensity profile, the experimental image contrast was estimated to be approximately 20%. Since the calculation is for the ideal case, the obtained contrast of 20% is fairly reasonable considering the fact that the absorption-contrast image shows little contrast. Fig. 6 demonstrates the high feasibility of the phase-contrast microscopy for observing transparent samples.

6. Conclusions

We have constructed an imaging transmission hard X-ray microscope at beamline BL24XU of SPring-8. Since both a wide field of view and a high spatial resolution have been achieved, the present microscopy will be applicable to observing practical samples. Further, the feasibility for observing transparent samples of light elements has been confirmed using Zernike's phase contrast method, and therefore the present microscopy will also be applicable for studying natural biological specimens without any sample preparations.

References

Awaji, M., Suzuki, Y., Takeuchi, A., Takano, H., Kamijo, N., Tamura, S. & Yasumoto, M. (2001). *Nucl. Instrum. Methods A*, **467/468**, 845–848.
Born, M. & Wolf, E. (1986). *Principles of Optics*, 6th ed. Oxford: Pergamon Press.
Henke, B. L., Gullikson, E. M. & Davis, J. C. (1993). *Atom. Data Nucl. Data Tables*, **54**, 181–342.
Lai, B., Yun, W., Xiao, Y., Yang, L., Legnini, D., Cai, C., Krasnoperova, A., Cerrina, F., Di Fabrizio, E., Grella, L. & Gentili, M. (1995). *Rev. Sci. Instrum.* **66**, 2287–2289.
Leitenberger, W., Weitkamp, T., Drakopoulos, M., Snigireva, I. & Snigirev, A. (2000). *Opt. Commun.* **180**, 233–238.
Lengeler, B., Schroer, C. G., Richwin, M., Tümmler, J., Drakopoulos, M., Snigirev, A. & Snigireva, I. (1999). *Appl. Phys. Lett.* **74**, 3924–3926.
Kagoshima, Y., Aoki, S., Kakuchi, M., Maezawa, H. & Ando, M. (1990). *Jpn. J. Appl. Phys.* **29**, L172–L174.
Kagoshima, Y., Ibuki, T., Takai, K., Yokoyama, Y., Miyamoto, N., Tsusaka, Y. & Matsui, J. (2000). *Jpn. J. Appl. Phys.* **39**, L433–L435.
Kagoshima, Y., Ibuki, T., Yokoyama, Y., Tsusaka, Y., Matsui, J., Takai, K. & Aino, M. (2001). *Jpn. J. Appl. Phys.* **40**, L1190–L1192.
Kaulich, B., Oestreich, S., Salome, M., Barrett, R., Susini, J., Wilhein, T., Di Fabrizio, E., Gentili, M. & Charalambous, P. (1999). *Appl. Phys. Lett.* **75**, 4061–4063.
Kinoshita, K., Matsumura, T., Inagaki, Y., Hirai, N., Sugiyama, M., Kihara, H., Watanabe, N. & Shimanuki, Y. (1992). *Proc. SPIE*, **1741**, 287–293.
Kohmura, Y., Awaji, M., Suzuki, Y., Ishikawa, T., Dudchik, Yu. I., Kolchevsky, N. N. & Komarov, F. F. (1999). *Rev. Sci. Instrum.* **70**, 4161–4167.
Kohmura, Y., Okada, K., Takeuchi, A., Takano, H., Suzuki, Y., Ishikawa, T., Ohigashi, T. & Yokosuka, H. (2001). *Nucl. Instrum. Methods A*, **467/468**, 881–883.
Ozawa, A., Tamamura, T., Ishii, T., Yoshihara, H. & Kagoshima, Y. (1997). *Microelectron. Eng.* **35**, 525–529.
Rudolph, D., Schmahl, G. & Niemann, B. (1990). *Modern Microscopies, Techniques and Applications*, edited by A. Michette & P. Duke, pp. 59–67. London: Plenum Press.
Schmahl, G., Rudolph, D., Guttmann, P., Schneider, G., Thieme, J. & Niemann, B. (1995). *Rev. Sci. Instrum.* **66**, 1282–1286.
Snigirev, A. (1995). *Rev. Sci. Instrum.* **66**, 2053–2058.
Takano, H., Suzuki, Y., Uesugi, T., Takeuchi, A. & Yagi, N. (2001). *Proc. SPIE*, **4499**, 126–133.
Tsusaka, Y., Yokoyama, K., Takai, K., Takeda, S., Kagoshima, Y. & Matsui, J. (2001). *Nucl. Instrum. Methods A*, **467/468**, 670–673.
Watanabe, N., Aoki, S., Takano, H., Yamamoto, K., Takeuchi, A., Tsubaki, H. & Aota, T. (2000). *X-ray Microscopy*, edited by W. Meyer-Ilse, T. Warwick & D. Attwood, pp. 84–91. New York: American Institute of Physics.
White, D. L., Wood, O. R. II, Bjorkholm, J. E., Spector, S., MacDowell, A. A. & LaFontaine, B. (1995). *Rev. Sci. Instrum.* **66**, 1930–1933.